JMEPEG (2012) 21:1141–1150
DOI: 10.1007/s11665-011-9985-1

1059-9495/$19.00

Modeling the Effects of Coolant Application in Friction Stir Processing on Material Microstructure Using 3D CFD Analysis

Sharif Aljoaba, Oscar Dillon Jr., Marwan Khraisheh, and I.S. Jawahir

(Submitted July 10, 2010; in revised form February 15, 2011)

The ability to generate nano-sized grains is one of the advantages of friction stir processing (FSP). However, the high temperatures generated during the stirring process within the processing zone stimulate the grains to grow after recrystallization. Therefore, maintaining the small grains becomes a critical issue when using FSP. In the present reports, coolants are applied to the fixture and/or processed material in order to reduce the temperature and hence, grain growth. Most of the reported data in the literature concerning cooling techniques are experimental. We have seen no reports that attempt to predict these quantities when using coolants while the material is undergoing FSP. Therefore, there is need to develop a model that predicts the resulting grain size when using coolants, which is an important step toward designing the material microstructure. In this study, two three-dimensional computational fluid dynamics (CFD) models are reported which simulate FSP with and without coolant application while using the STAR CCM+ CFD commercial software. In the model with the coolant application, the fixture (backing plate) is modeled while is not in the other model. User-defined subroutines were incorporated in the software and implemented to investigate the effects of changing process parameters on temperature, strain rate and material velocity fields in, and around, the processed nugget. In addition, a correlation between these parameters and the Zener-Holloman parameter used in material science was developed to predict the grain size distribution. Different stirring conditions were incorporated in this study to investigate their effects on material flow and microstructural modification. A comparison of the results obtained by using each of the models on the processed microstructure is also presented for the case of Mg AZ31B-O alloy. The predicted results are also compared with the available experimental data and generally show good agreement.

Keywords advanced characterization, heat treating, modeling processes, modification, non-ferrous metals

1. Introduction

On observing the advantages associated with friction stir welding (FSW), mainly grain refinement, the phenomenon has been applied to the processing of larger sheets commercial alloys. Friction stir processing (FSP) is a solid-state process in which a specially designed rotating cylindrical tool, consisting of a pin and a shoulder, is plunged into the sheet specimen being processed. The tool is then moved in the desired direction (Fig. 1). The rubbing of the rotating shoulder generates heat which softens the material (while keeping the temperature below the melting point) and with the mechanical stirring caused by the pin, the material within the processed zone undergoes intense plastic deformation yielding a dynamically recrystallized fine-grain structure. Despite being a solid-state process, FSP is modeled using CFD in order to study the velocity and motion of the material during the stirring process. Several researchers (Ref 1-5) have previously used computational fluid dynamics (CFD) to simulate FSP. They assumed the FS-processed material to be a non-Newtonian fluid. They used different CFD codes to determine velocity fields, material flow, and temperature distributions. Other researchers (Ref 6-12) used finite element analysis, visco-plastic and analytical models, to determine temperature and strain rate fields.

Despite of using high hardness and heat-treated materials for the FSP tools, abrasive wear phenomenon occurs due to the stirring action, friction, and the high strain rates taking place in the processing zone. This phenomenon is characterized by the reduction in the height and diameter of the tool's pin and abrasive debris. Some efforts were found focusing on studying this phenomenon. Contorno et al. (Ref 13) conducted experimental work in order to study this phenomenon. They used AlSiCrN and AlSiTiN nano-composite coatings on a AISI 1040 steel trimmed tool pin to process Al 359 + 20% SiC metal matrix composites (MMC). They observed that, at least on the basis of their investigations, there is no definitive advantage of the coatings on the hardened tool. Their obtained results state that tools used for FSP operations on MMC materials must be manufactured with specific accuracy. This helps avoiding any brittle behavior at the beginning of the tool working life, where cracks and strong stress concentrations must be definitively preserved. Fernandez and Murr (Ref 14) conducted an experimental investigations of using threaded steel tool pin cut from

Sharif Aljoaba, Mechanical Engineering Department, University of Kentucky, 453 F. Paul Anderson Tower, Lexington, KY 40506-0046; **Oscar Dillon Jr.** and **I.S. Jawahir**, Mechanical Engineering Department, University of Kentucky, 414B CRMS Building, Lexington, KY 40506; and **Marwan Khraisheh**, Masdar Institute of Science and Technology, Abu Dhabi, UAE. Contact e-mails: szaljo2@engr.uky.edu, vzn05xpm@verizon.net, jawahir@engr.uky.edu, and mkhraisheh@masdar.ac.ae.

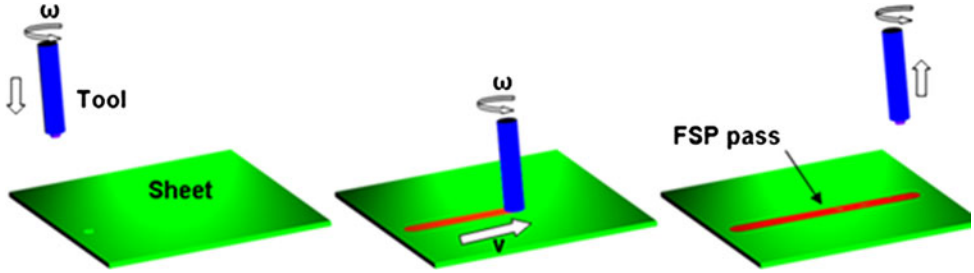

Fig. 1 Schematic of friction stir processing steps (Ref 20)

a 1/4-20, 01 AISI oil-hardened to FSW of Al 359 + 20% SiC MMC. They observed that the threaded steel tool pins wear significantly at the high rotation speeds and slow weld traverse speeds. However, as the tool rotation speed is reduced and the weld traverse speed is increased, the tool wear initially declines because the threads fill with work-piece material. Further, they obtained that as the tool threads begin to wear away, the actual tool wear declines except at some large weld traverse lengths (larger than 3 m), the tool pin is shaped into a smooth optimized shape. After this smooth optimized shape took place, no tool wear was observed. They concluded that this phenomenon results by variations in the complex solid-state flow as welding progresses. Furthermore, they found that welds made after the tool pin is optimally shaped are more homogeneous and there is very little SiC particle comminuting.

The focus of this research as mentioned previously is to simulate the effects of the cooling application during the FSP on the produced grain sizes. Since, the used flat tool pin is made of H13 tool steel which is of much higher yielding strength than the processed material (Mg Az31B-O); this phenomenon might not be significantly involved. However, this simulation can also be used to study the effects of cooling on the tool wear. This can be accomplished by comparing the temperature distribution, strain rate, and flow stresses of the FSP tool at different rotational speeds with and without coolant application. However, this will be considered in a future work since it is not the focus of this study.

In general, most of the CFD work that has been done to simulate FSP, or FSW, uses two-dimensional models and neglects the dependency of material properties on either temperature, strain rate, or both. Still, there is a great need for a comprehensive 3D model which can accurately simulate the actual FSP/FSW process. Recent results (Ref 15-18) show that an optimally developed FSP can produce the desired nano-sized grains in the worked materials. It has been found that if the temperature is kept within the recrystallization temperature range of the material during the process, nano-size grain structure can be obtained. In a previous work (Ref 19), a three-dimensional CFD model was developed to simulate FSP using the STAR CCM+ CFD commercial software. This study presents a comparison between results of two CFD models, one with and one without the application of coolant to the fixture during the FSP of Mg AZ31B-O alloy.

2. CFD Models Description

The simulation is based on solving continuity, momentum, and energy equations. STAR CCM+ uses the finite volume method to solve these equations for each cell in the mesh, where polyhedral cell is used to build up the model's mesh due to the complexity of the geometries. Initial and boundary conditions (BC) were defined based on the experimental work conducted by Darras (Ref 20) and the author (Ref 21), and some simplifying assumptions. The CFD code automatically uses convectional heat transfer BC for the interfaces, and the coefficient of heat transfer is also automatically calculated because it considers the complexity of all of the convection, conduction, and radiation heat transfer coefficients at the interfaces. The top and bottom of the sheet were assumed to lose heat to the surroundings through convection. At the sides of the sheet, a fixed temperature BC was assumed, which was taken to be equal to room temperature since the sheet is considered to be thin.

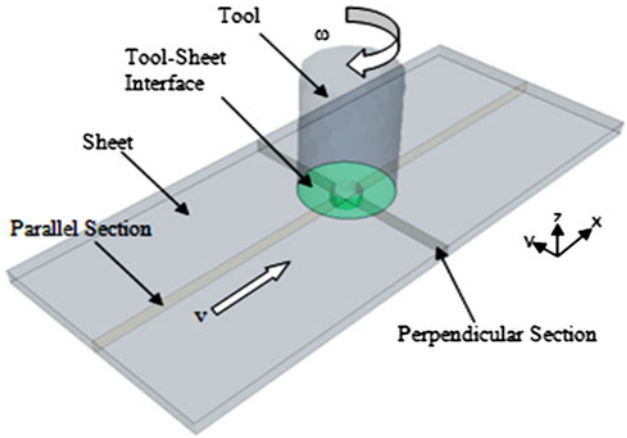

Fig. 2 CFD model without coolant application (Ref 12)

The first model (without coolant, Fig. 2) consists of two bodies; the first one is the tool, which is assumed to be a rigid solid body. The second one is the sheet, which is assumed to be a non-Newtonian fluid (i.e., the viscosity is not constant) while demonstrating actual sheet-material properties, moves with the desired translational velocity (v, m/s). An interface between the tool and the sheet was created, and it was assumed that each point on the interface has the same velocity as its corresponding point on the tool.

The second 3D CFD model (with coolant) is built in order to simulate FSP combined with external cooling. As shown in Fig. 3, the model consists of four bodies: tool, sheet (the same as in the first model), third is the backing plate which is assumed to be solid having the properties of AISI 4142 alloy steel, and fourth is a straight cooling channel. For the coolant channel, a mass flow and pressure BCs were used for its inlet and the outlet, respectively. The fluid flows through the cooling

channel in the backing plate as shown in Fig. 4. This fluid has the coolant properties, and in this model the applied coolant is water at room temperature (295-298 K).

A constant density and steady state condition using the segregated solid energy method is applied to the tool. In this study, since the flow of sheet's material and the coolant were assumed incompressible and the time and the computational capabilities are important factors the segregated approach is used. The major assumptions that have been made are constant density, laminar flow, and steady state conditions for the sheet and the coolant.

Since the sheet mentioned is modeled as a non-Newtonian fluid, several user-defined functions were introduced to calculate the dynamic viscosity of the material, which is mainly a function of local values of temperature and strain rate, making the model visco-plastic. Furthermore, user-defined functions were developed and implemented to investigate the effects of the process parameters on temperature, strain rate, flow stress, and material velocity fields in and around the processed nugget. Additional derived parameters were computed in order to predict the grain size distribution in the processed zone. The Zener-Holloman parameter, Z, is the major metric that is needed for these computations. The following formulations of flow stress, Zener-Holloman parameter, and dynamic viscosity, are proposed by Sheppard and Wright (Ref 22):

$$\sigma_e = \frac{1}{\alpha}\sinh^{-1}\left[\left(\frac{Z}{A}\right)^{1/n}\right] \quad \text{(Eq 1)}$$

$$Z = \varepsilon \exp\left(\frac{Q}{RT}\right) \quad \text{(Eq 2)}$$

$$\mu = \frac{\sigma_e}{3\dot{\varepsilon}}, \quad \text{(Eq 3)}$$

where A, α, and n are material constants. Q is the activation energy of lattice diffusion of the sheet's material, R is the gas constant, and $\dot{\varepsilon}$ is the effective strain rate. σ_e is the flow stress, and μ is dynamic viscosity, which can be noticed to be completely defined by the temperature and the strain rate. Values of A, α, n, and Q of the AZ31 magnesium alloy are shown in Table 1, while its composition is shown in Table 2.

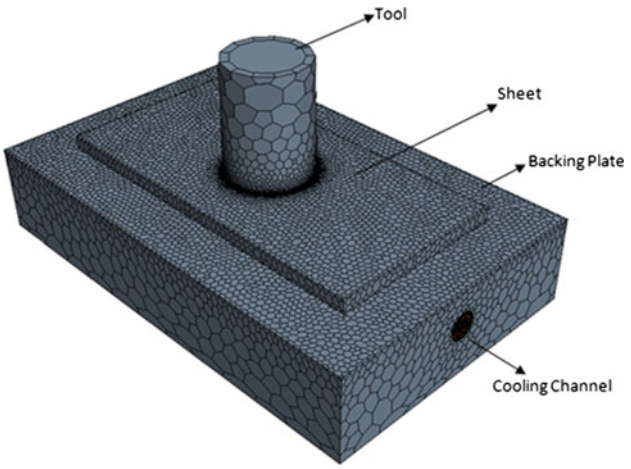

Fig. 3 CFD model with coolant channel

Table 1 Data of Mg AZ31 and H13 tool steel used in the CFD simulation

Properties and constants	Value
Sheet material density (Ref 24)	1777 kg/m^3
Specific heat (Ref 24)	$0.2441 + 105e - 6T - 2783T^{-2}$
Thermal conductivity (Ref 24)	96 W/m K
Liquidus temperature (Ref 24)	903 K
Solidus temperature (Ref 24)	878 K
Activation energy Q (Ref 25)	130 kJ/mol
Material constant A (Ref 25)	2.75E7 s^{-1}
Material constant n (Ref 25)	1.8
Material constant α (Ref 25)	0.052 MPa^{-1}
Gas constant R (Ref 25)	8.314472 J/K mol
Tool material density (Ref 24)	7800 kg/m^3
Specific heat (Ref 24)	460 J/Kg K
Thermal conductivity (Ref 24)	24.3 W/m K
Coefficient of friction used (μ_f) (Ref 26)	0.4
Zener-Holloman-grain size (Ref 23)	$\ln d = 9.0 - 0.27 \ln Z$

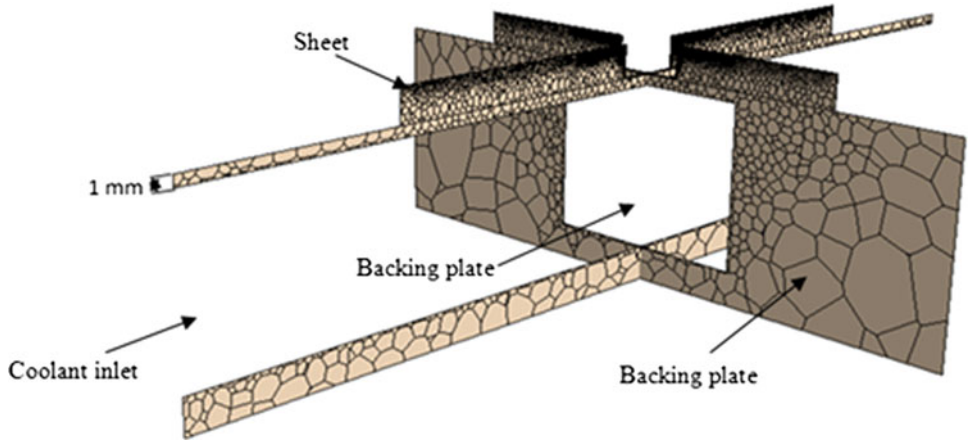

Fig. 4 Cross sections through the model

3. Results and Discussion

The model was built with a flat tool pin geometry that has a 6.4 mm (0.25 in.) pin diameter, 3.1 mm pin height, and 19.1 mm (0.75 in.) shoulder diameter. The tool material is H13 tool steel. The selected sheet material was the AZ31B-O magnesium alloy, the thickness of which was chosen to match a commercially available size. The modeled sheet is 12 cm long, 5 cm wide, and 3.2 mm thick. All data used in the analysis are shown in Table 1. The simulation is conducted for a constant translational speed of 12 ipm, and different rotational speeds of 1000, 1200, and 1750 rpm. These values were selected in order to be the same as the ones used experiments.

3.1 Predicted Temperature Fields

The calculated temperature contours for different stirring conditions are shown in Fig. 5. It was noticed that as the tool's rotational speed increased predicted temperatures increased. It was also observed that the temperature of the stirred material increased with increasing radial distance toward the tool's outer edge. This is expected since the material there has higher velocity of deformation due to its position: the velocity is highest at the shoulder's edges, and accordingly the material in that region has higher friction and plastic deformation.

Table 2 Composition of Mg AZ31B-O alloy (Ref 27)

Component	Wt.%
Aluminum, Al	2.50-3.50
Calcium, Ca	Max. 0.040
Copper, Cu	Max. 0.050
Iron, Fe	Max. 0.0050
Magnesium, Mg	97.0
Manganese, Mn	Max. 0.20
Nickel, Ni	Max. 0.0050
Silicon, Si	Max. 0.10
Zinc, Zn	0.60-1.40

The contours are shaped like onion rings and show a difference in the temperature distributions between zones lying before and after the tool pin. There was also a small difference between the temperatures at the advancing and the retreating sides of the tool. Figure 5(c) shows that the highest temperature is approximately 1000 K, which exceeds the melting point of the material. This is due to the very high rotational speed (1750 rpm), which was sufficient to cause localized melting of the material, as also verified experimentally (Ref 20, 21).

The simulation results of the CFD model with coolant application are found for two mass flow rates, 0.5 and 1 kg/s as shown in Fig. 6 and 7. As expected, the maximum temperature is still at the tool's shoulder, and it is comparable to the temperature values without cooling application. However, the temperature values obtained at zones close to the bottom of the sheet (Zone A) are smaller in case of coolant application than without coolant application, and it is close to the recrystallization temperature of the magnesium (500 K). This is due to the amount of heat that is removed by the coolant.

In addition, as shown in Fig. 7, the temperature in the zones close to the bottom of the sheet is lower than those shown in Fig. 6, which is a result of using different coolant's mass flow rate. This can be noticed in the difference of the green color intensity, where it is higher in case of 0.5 kg/s than the 1 kg/s coolant flow rate.

3.2 Predicted Strain Rate

Strain rate has always been difficult to measure experimentally. However, STAR CCM+ tools provide the ability to calculate the strain rate everywhere in the process using Eq. 4 and 5.

$$S = |\mathbf{W}| = \sqrt{2\mathbf{W} : \mathbf{W}^T}, \quad \text{(Eq 4)}$$

where the vorticity tensor $\mathbf{W}$ is defined as:

$$\mathbf{W} = \frac{1}{2}(\nabla \mathbf{v} - \nabla \mathbf{v}^T), \quad \text{(Eq 5)}$$

where v is the velocity vector and T is the transpose.

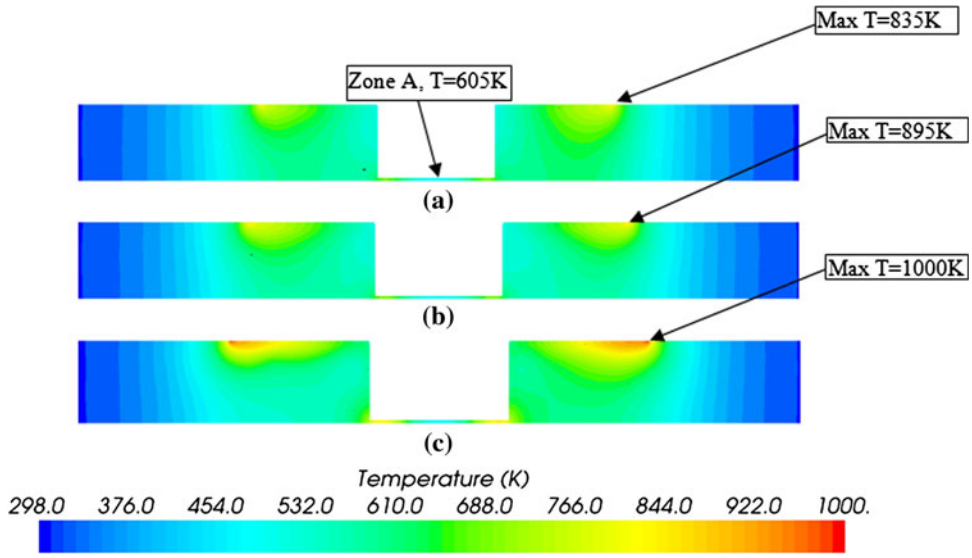

Fig. 5 Simulated temperature distribution in the sheet for flat tool pin geometry at rotational speeds of (a) 1000, (b) 1200, and (c) 1750 rpm

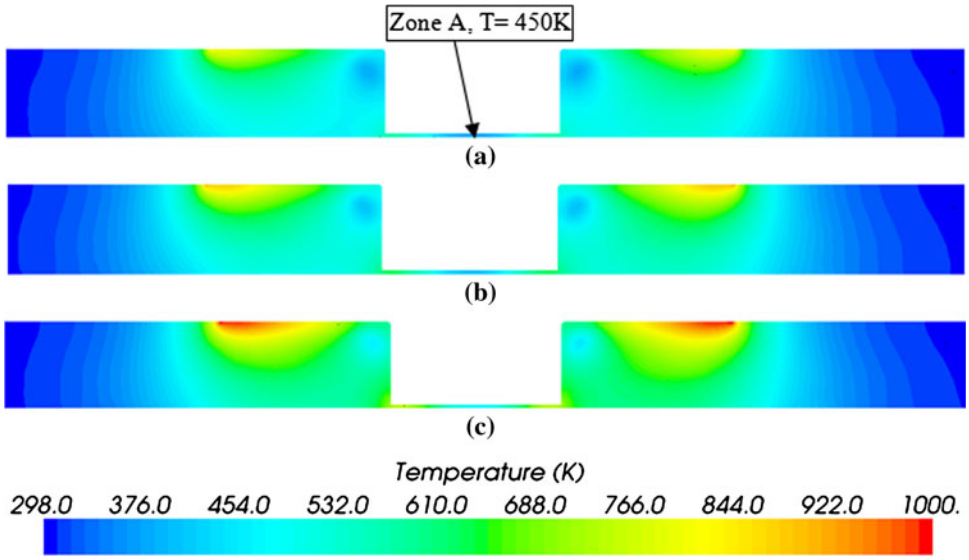

Fig. 6 Simulated temperature distribution at 0.5 kg/s of coolant mass flow rate and at rotational speeds of (a) 1000, (b) 1200, and (c) 1750 rpm

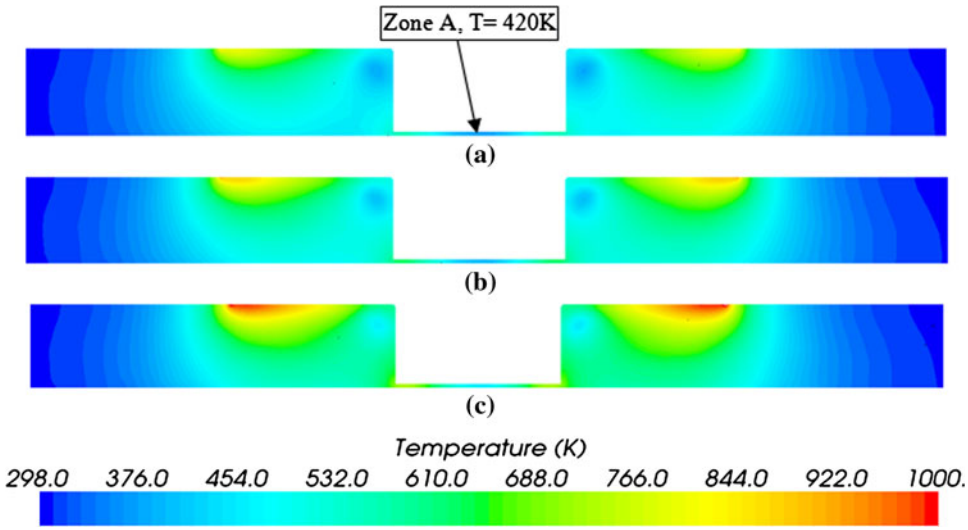

Fig. 7 Simulated temperature distribution at 1 kg/s of coolant mass flow rate and at rotational speeds of (a) 1000, (b) 1200, and (c) 1750 rpm

Figures 8-10 show the predicted strain rate values and their distributions with and without coolant application. It is observed that the strain rate is highly influenced by the rotational speed, and increases along with it. The highest values are in the contact zone with the outer edge of the tool's shoulder, where the temperature and the material speed are the highest.

The difference in the values between the results of coolant application and those without coolant can be clearly noticed, where the strain rate at zone B is 1300 s^{-1} with coolant application, while at the same zone it is 400 s^{-1} when there is no coolant application. Hence, the strain rate has much higher values with coolant application than without. Furthermore, strain rate has higher values in case of 1 kg/s than the 0.5 kg/s flow rate, where at zone A for the 0.5 kg/s coolant flow rate, strain rate is 1300 s^{-1} while it is 1850 s^{-1} for 1 kg/s coolant flow rate. It can also be distinguished through the difference in the intensity of the colors, where more intensive color means higher values.

Some researchers (Ref 23) have developed a model to calculate the strain rate using assumed geometrical constants. Equation 6 (Ref 23) provides a relation used to calculate the strain rate:

$$\dot{\varepsilon} = \frac{R_m \cdot 2\pi\gamma_e}{L_e}, \qquad \text{(Eq 6)}$$

R_m is the average material flow rate, γ_e and L_e are the radius and the depth of the recrystallized zone, respectively. According to the estimated values of these constants, the values of the strain rate are found small [for 800 and 1800 rpm, the strain rate is 24 and 50 s^{-1}, respectively (Ref 23)] compared to the predicted values using the CFD analysis. Hence, these predicted strain rate values can be used in Eq 6 to calculate the constants that have been assumed in order to give more accurate results. In addition, it has been noticed that it is so difficult for a non-expert to understand the method by which the values of these constants were determined, or estimated. Furthermore, this relationship calculates the average value of

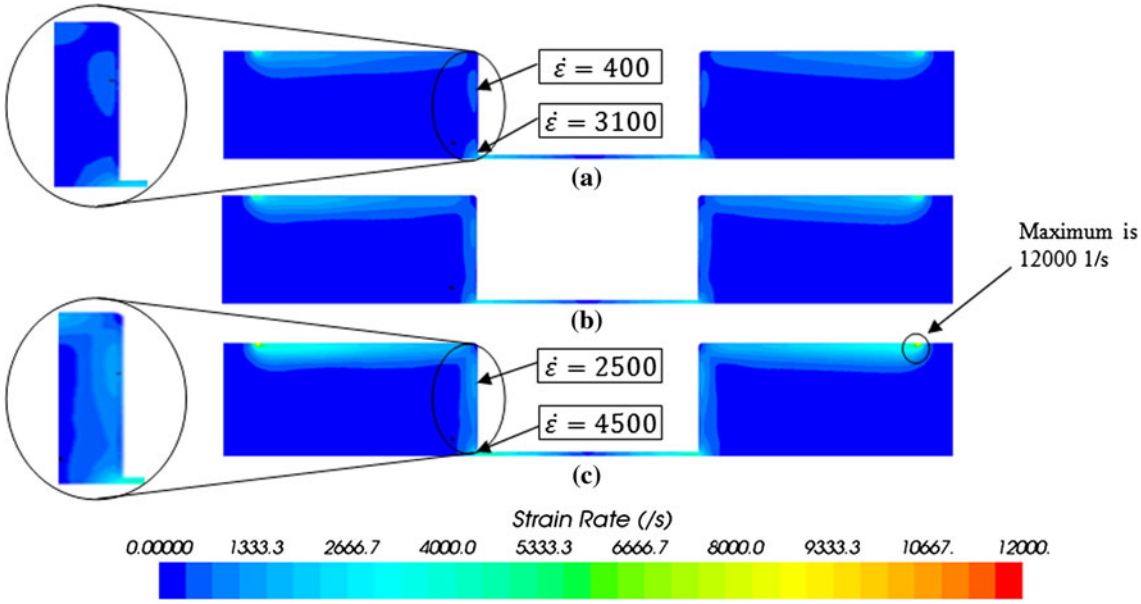

Fig. 8 Simulated strain rate values in the sheet for flat tool pin at rotational speeds of (a) 1000, (b) 1200, and (c) 1750 rpm

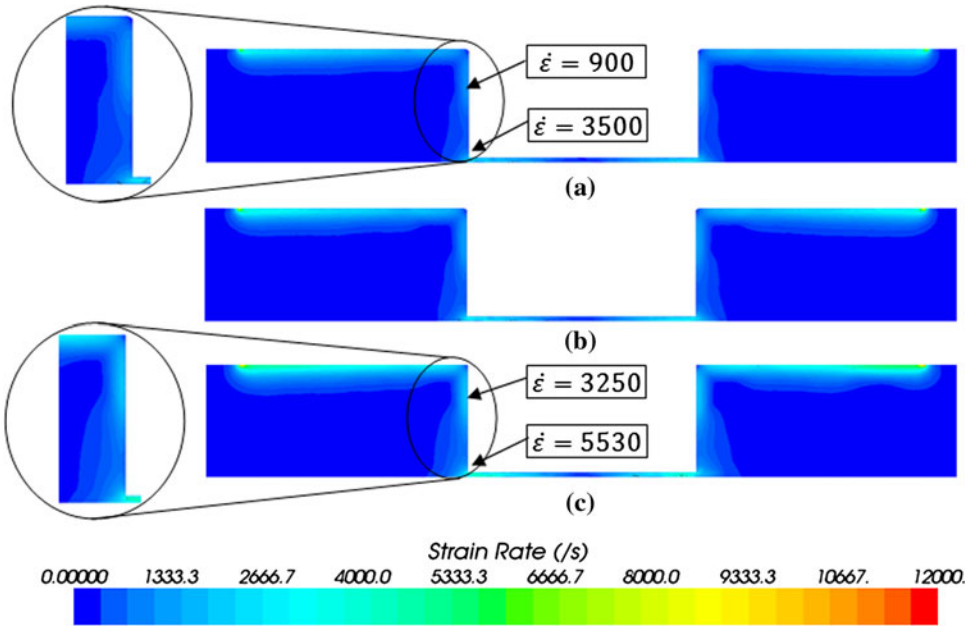

Fig. 9 Strain rate values at 0.5 kg/s of coolant mass flow rate and at rotational speeds of (a) 1000, (b) 1200, and (c) 1750 rpm

the produced strain rate, while the strain rate has a wide range of values where the minimum and maximum values have a huge difference. Hence, such a simple formulas are not so good in predicting the strain value. On the other hand, as shown in Fig. 8, 9, and 10, the strain rate values are distributed across the processing zone, where it is maximum, minimum, and generic values can be obtained. Moreover, it has been noticed in these figures also that the coolant has an effect on the strain rate values, while the temperature (or coolant) effect is does not explicitly appear in this formulation.

3.3 Predicted Grain Size

Grain size after recrystallization is determined using an empirical relationship (Eq 7) that relates it to the Zener-Holloman parameter. The relationship was developed specifically for AZ31 magnesium alloy by Darras (Ref 20), who used experimental measurements of the average grain size (d, μm) and temperature of the processed alloy for the same stirring conditions [see also Chang et al. (Ref 23), who's equation is shown in Table 1]. He then calculated the Zener-Holloman

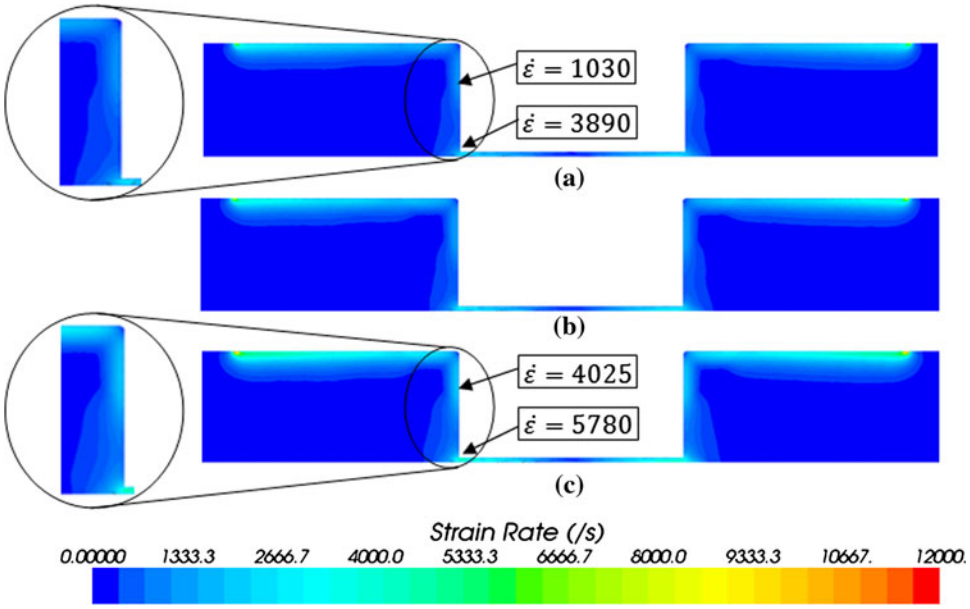

Fig. 10 Strain rate values at 1 kg/s of coolant mass flow rate and at rotational speeds of (a) 1000, (b) 1200, and (c) 1750 rpm

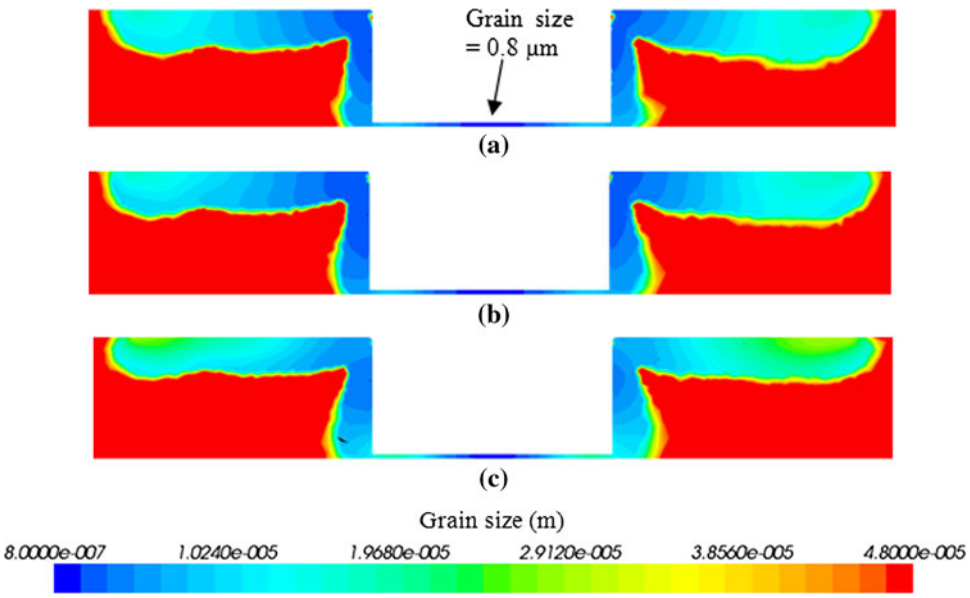

Fig. 11 Calculated grain size distribution in the sheet for FSP with flat tool pin at rotational speeds of (a) 1000, (b) 1200, and (c) 1750 rpm

parameter using Eq 2 and obtained the constants of the linear relationship.

$$\ln\ d = 8.65 - 0.21\ \ln Z \qquad \text{(Eq 7)}$$

This equation has only been applied to the process zone, where grain size is changing and not in other areas. In order to determine this zone, its boundaries are determined by specifying the temperature and strain rate value constraints. These constraint values are temperature is higher than 500 K [temperature range for recrystallization of the magnesium alloy is 523-753 K (Ref 20)]; and strain rate is larger than 0.5 (s^{-1}). The grain size for other non-processing zones is artificially assumed to remain at its initial value of 48 μm in order to show better contrast between the processed and non-processed zones.

Figure 11 shows the distribution of the predicted grain size without coolant application. It is observed that as the rotational speed increases, the grain size increases. This is due to the effect of increased temperature on grain growth. In other words, grain size has the same pattern for different rotational speeds, but with different values. The average grain size at the advancing side of the stirring zone is smaller than that in the retreating side; and the grain size in front of the tool is smaller than that at the rear side of the tool in that zone. This is again supported by the dissimilarity in temperature distributions in these zones.

In Fig. 11, it can be seen that the average grain size at the top of the processed zone is larger than those at lower levels (closer to the bottom of the processed zone). This is likely

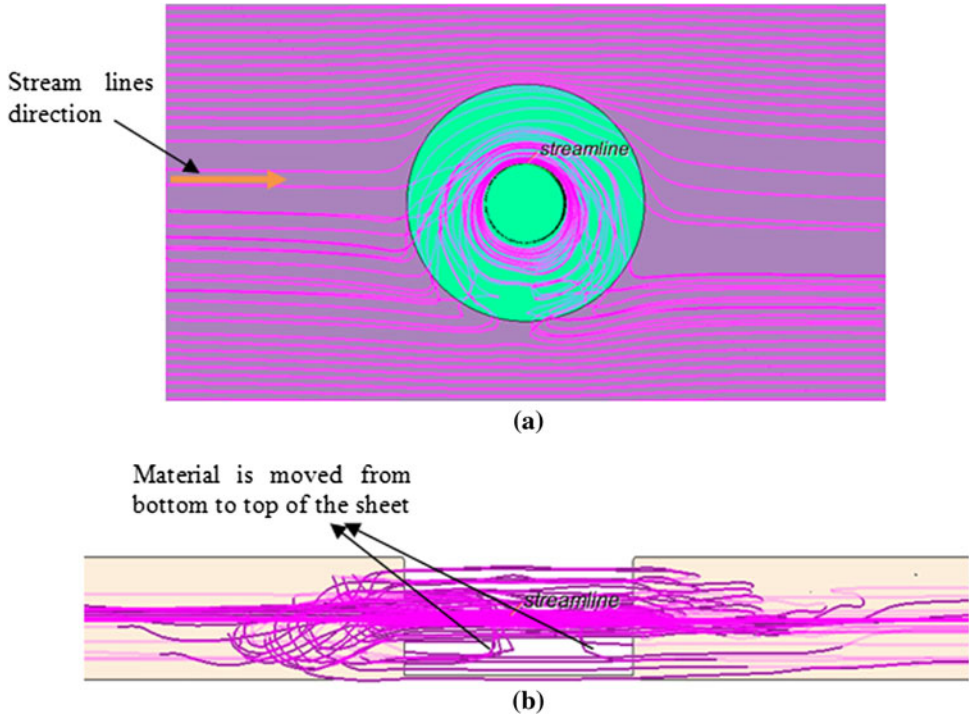

Fig. 12 Material flow around the tool at 1000 rpm and 12 ipm. (a) Stream lines simulate the material flow and (b) stream lines simulates the material flow through thickness cross section

Table 3 Average experimental grain size for Mg AZ31B-O alloy, FS-processed samples (Ref 20)

FS processed at		Average grain size, μm
Rotational speed, rpm	Translational speed, in./min	
1000	12	5.2
1200	12	6.1
1750	12	8.1

due to the higher temperature values at the top, which promotes the grain growth. In addition, the grain size has the smallest value, which is close to 800 nm, at the bottom of the sheet (contact zone with the pin surface). This can be attributed to the following scenario. Since the smallest grains are recrystallized at the bottom of the sheet, these grains will be moved up through sheet's thickness due to the stirring action. This action is shown in Fig. 12(a) and 12(b), after an extensive study, it has been noticed that the grains are moved up close to the sheets surface and due to the high temperature there (closer to surface); the grains growth occurs for these grains. The average grain size values of the CFD code of this model showed good agreement with the experimental data obtained by Darras (Ref 20) for the same material and same stirring conditions as shown in Table 3, which verifies the model.

Figures 13 and 14 show the calculated grain size of the sheets processed with coolant applied to the fixture at two mass flow rates, i.e., 0.5 and 1 kg/s, respectively. The as-received grain size sheet that is used in the experiments is 10 μm.

It can be seen that the grains are refined close and into the nugget zone and in zones close to the bottom of the sheet, while the grains are larger in the zones close to the tool's shoulder. This is due to the high temperature there, and the coolant does not reach this region and therefore cannot have a significant effect there. However, the applied coolant significantly affects the bottom of the sheet. As shown, the smallest grain size occurs at the bottom of the sheet where the pin of the tool stirring the material, and the produced temperature is reduced by the coolant. If it is compared with the results shown in Fig. 11, it can be seen that both (with and without coolant) have the smallest predicted grain size at the bottom, but in case of coolant application as shown, the smallest grain size is 260 nm while it is 800 nm without coolant application. These values of the grain size were calculated during the process, and they may change after the tool passes by (i.e., during cooling the sheet down to room temperature).

4. Summary

In this study, a 3D CFD model is created in order to simulate FSP with and without coolant application. The significant contribution in this study is the ability of estimating the grain size of the processed material as a step toward optimizing the process for better material processing and for more sustainable manufacturing applications. Furthermore, the following results were demonstrated:

1. FSP is a new innovative sustainable (no external heating source required, and no toxic wastes/emissions) microstructural modification technique for achieving

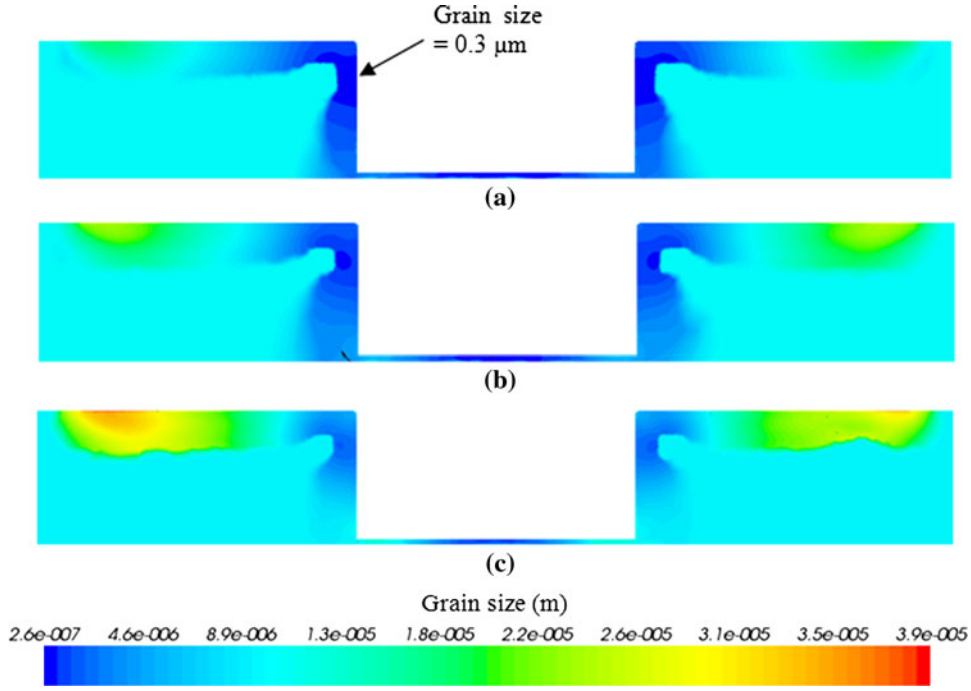

Fig. 13 Calculated grain size at 0.5 kg/s of coolant mass flow rate and at rotational speeds of (a) 1000, (b) 1200, and (c) 1750 rpm

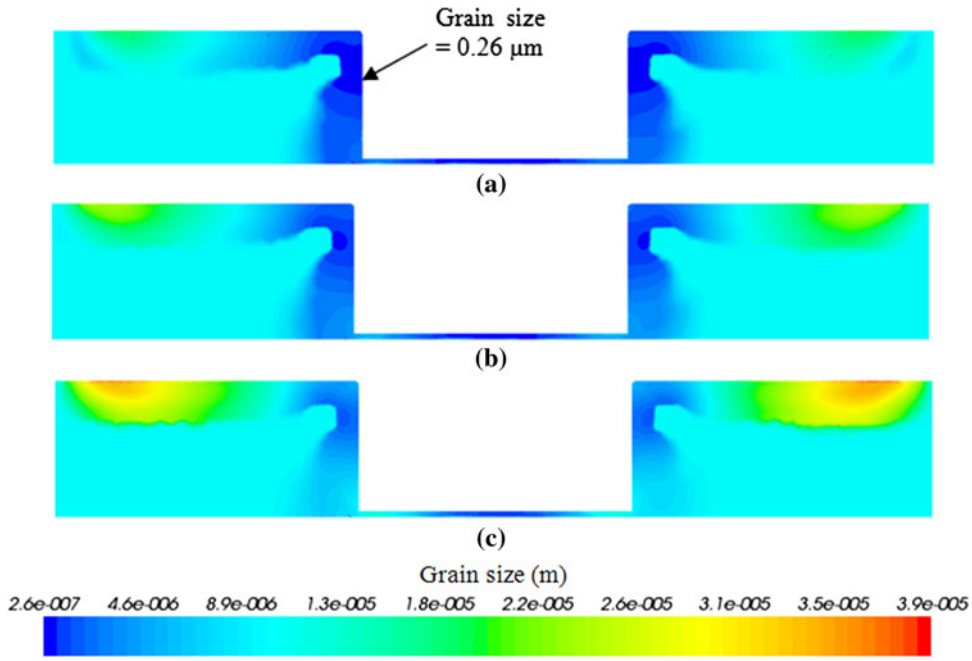

Fig. 14 Calculated grain size at 1 kg/s of coolant mass flow rate and at rotational speeds of (a) 1000, (b) 1200, and (c) 1750 rpm

homogeneous fine-grain structure in materials especially for the light-weight alloys.

2. Stirring conditions (rotational and translational speeds) significantly affect the process and the resulting grain structure, and are different for different materials. In this research, a range of stirring conditions that provide good processed material quality (defect free) and small grains for AZ31B magnesium alloy.
3. Controlling the temperature in the processing zone within the crystallization temperature of the material is important to producing nano-size grain sheets. Applying coolants during the process assists in this process.
4. CFD is a useful tool to simulate FSP and provides a good estimate for the material behavior during the process. It also helps in designing the process parameters (stirring conditions, experimental tools, and equipments) that provide the desired fine-grain structure.
5. The results obtained from CFD can be used to verify the relations those have been used to determine strain rate which is used to determine Zener-Holloman parameter,

and accordingly the grain size. Such relations were used to give results based on constants which their values were assumed.

References

1. P. Colegrove and H.R. Shercliff, 3-Dimensional CFD Modeling of Flow Round a Threaded Friction Stir Welding Tool Profile, *Mater. Process. Technol.*, 2005, **169**, p 320–327
2. T. Hyoe, P.A. Colegrove, and H.R. Shercliff, Thermal and Microstructure Modeling in Thick Plate Aluminum Alloy 7075 Friction Stir Welds, *Friction Stir Welding and Processing II*, TMS (The Minerals, Metals & Materials Society), 2003
3. H. Schmidt and J. Hattel, CFD Modeling of the Shear Layer Around the Tool Probe in Friction Stir Welding, *Friction Stir and Processing III*, TMS, 2005, p 225–232
4. P. Colegrove and H. Sherchiff, 2-Dimensional CFD Modeling of Flow Round Profiled FSW Tooling, *Friction Stir Welding and Processing II*, TMS, 2003, p 13–23
5. T. Long, T. Seidel, W. Tang, and A. Reynolds, A Friction Stir Welding Model Using Computational Fluid Dynamics, Hot Deformation of Aluminum Alloys III, *TMS Annual Meeting*, San Diego, 2003, p 299–312
6. H. Zhang, Z. Zhang, and J. Chen, 3D Modeling of Material Flow in Friction Stir Welding Under Different Process Parameters, *J. Mater. Process. Technol.*, 2007, **183**, p 62–70
7. G. Buffa, J. Hua, R. Shivpuri, and L. Fratini, Design of the Friction Stir Welding Tool Using the Continuum Based FEM Model, *Mater. Sci. Eng. A*, 2006, **419**, p 381–388
8. G. Buffa, J. Hua, R. Shivpuri, and L. Fratini, A Continuum Based FEM Model for Friction Stir Welding-Model Development, *Mater. Sci. Eng. A*, 2006, **419**, p 389–396
9. P. Ulysse, Three-Dimensional Modeling of Friction Stir-Welding Process, *Int. J. Mach. Tools Manuf.*, 2002, **42**, p 1549–1557
10. C.M. Chen and R. Kovacevic, Finite Element Modeling of Friction Stir Welding—Thermal and Thermomechanical Analysis, *Int. J. Mach. Tools Manuf.*, 2003, **43**, p 1319–1326
11. C. Chen and R. Kovacevic, Thermomechanical Modeling and Force Analysis of Friction Stir Welding by the Finite Element Method, *Proc. Inst. Mech. Eng. C J. Mech. Eng. Sci.*, 2004, **218**, p 17–33
12. B. Darras and M. Khraisheh, Analytical Modeling of Strain Rate Distribution During Friction Stir Processing, *J. Mater. Eng. Perform.*, 2008, **17**, p 168–177
13. D. Contorno, M.G. Faga, L. Fratini, L. Settineri, and G. Gautier di Confiengo, Wear Analysis During Friction Stir Processing of A359 + 20%SiC MMC, *Key Eng. Mater.*, 2009, **410–411**, p 235–244
14. G. Fernandez and L. Murr, Characterization of Tool Wear and Weld Optimization in the Friction-Stir Welding of Cast Aluminum 359 + 20% SiC Metal-Matrix Composite, *Mater. Charact.*, 2004, **52**, p 65–75
15. C. Chang, X. Du, and J. Huang, Achieving Ultrafine Grain Size in Mg-Al-Zn Alloy by Friction Stir Processing, *Scr. Mater.*, 2007, **57**, p 209–212
16. C. Rhodes, M. Mahoney, W. Bingel, and M. Calabrese, Fine-Grain Evolution in Friction-Stir Processed 7050 Aluminum, *Scr. Mater.*, 2004, **48**, p 1451–1455
17. C. Chang, X. Du, and J. Huang, Achieving Ultrafine Grain Size in Mg-Al-Zn Alloy by Friction Stir Processing, *Scr. Mater.*, 2008, **59**, p 356–359
18. X. Du and B. Wu, Using Two-Pass Friction Stir Processing to Produce Nanocrystalline Microstructure in AZ61 Magnesium Alloy, *Sci. China Ser. E Technol. Sci.*, 2009, **52**(6), p 1751–1755
19. S. Aljoaba, I. Jawahir, O. Dillon, M. Ali, and M. Khraisheh, Modeling of Friction Stir Processing Using 3D CFD Analysis, *Material Forming 12th ESAFORM Conference*, Netherlands, April 2009
20. B. Darras, "Integrated Thermo-Mechanical Investigations of Friction Stir Processing of Light Weight Alloys," PhD Theses, University of Kentucky, 2008
21. S. Aljoaba, "Experimental Investigation and Modeling of Friction Stir Processing Using 3D CFD Analysis," Master's Thesis, University of Kentucky, 2009
22. T. Sheppard and D. Wright, Determination of Flow Stress: Part 1 Constitutive Equation for Aluminum Alloys at Elevated Temperatures, *Met. Technol.*, 1979, **6**, p 215–223
23. C. Chang, C. Lee, and J. Huang, Relationship Between Grain Size and Zener-Holloman Parameter During Friction Stir Processing in AZ31Mg Alloys, *Scr. Mater.*, 2004, **51**, p 509–514
24. Anonymous, *ASM International Metals Handbook, ASM Handbook*, 10th ed., Vol 2, 1990, p 455
25. H.J. McQueen, M. Myshlaev, M. Sauerborn, and A. Mwembela, Flow Stress Microstructures and Modeling in Hot Extrusions of Magnesium Alloys, *Magnesium Technology 2000*, The Minerals, Metals and Materials Society, 2000, p 355–362
26. O. Frigaard, O. Grong, and O.T. Midling, A Process Model for Friction Stir Welding of Age Hardening Aluminum Alloys, *Metall. Mater. Trans. A*, 2001, **32**, p 1189–1200
27. Anonymous, Matweb LLC Website, Magnesium AZ31B-O Annealed Sheet, 2010, http://www.matweb.com/search/DataSheet.aspx?MatGUID=ac0c011a4d6a4948ac7b56c07f91b95f&ckck=1